Accepted Manuscript

Discovery of imidazoleisoindole derivatives as potent IDO1 inhibitors: Design, synthesis, biological evaluation and computational studies

Yi Zou, Fang Wang, Yan Wang, Qirui Sun, Yue Hu, Yuezhen Li, Wen Liu, Wenjie Guo, Zhangjian Huang, Yihua Zhang, Qiang Xu, Yisheng Lai

PII: S0223-5234(17)30739-0

DOI: 10.1016/j.ejmech.2017.09.025

Reference: EJMECH 9740

To appear in: *European Journal of Medicinal Chemistry*

Received Date: 25 March 2017

Revised Date: 20 August 2017

Accepted Date: 14 September 2017

Please cite this article as: Y. Zou, F. Wang, Y. Wang, Q. Sun, Y. Hu, Y. Li, W. Liu, W. Guo, Z. Huang, Y. Zhang, Q. Xu, Y. Lai, Discovery of imidazoleisoindole derivatives as potent IDO1 inhibitors: Design, synthesis, biological evaluation and computational studies, *European Journal of Medicinal Chemistry* (2017), doi: 10.1016/j.ejmech.2017.09.025.

Graphical abstract

Discovery of imidazoleisoindole derivatives as potent IDO1 inhibitors: Design, synthesis, biological evaluation and computational studies

Yi Zou [a,1], Fang Wang [a,1], Yan Wang [b,1], Qirui Sun [a], Yue Hu[b], Yuezhen Li [c], Wen Liu [b], Wenjie Guo [b,*], Zhangjian Huang [a], Yihua Zhang [a], Qiang Xu [b,*], Yisheng Lai [a,**]

[a]*State Key Laboratory of Natural Medicines, Jiangsu Key Laboratory of Drug Discovery for Metabolic Diseases, Center of Drug Discovery, China Pharmaceutical University, Nanjing 210009, China*

[b]*State Key Laboratory of Pharmaceutical Biotechnology, School of Life Sciences, Nanjing University, Nanjing 210093, China*

[c] *Department of Organic Chemistry, School of Science, China Pharmaceutical University, Nanjing 211198, China*

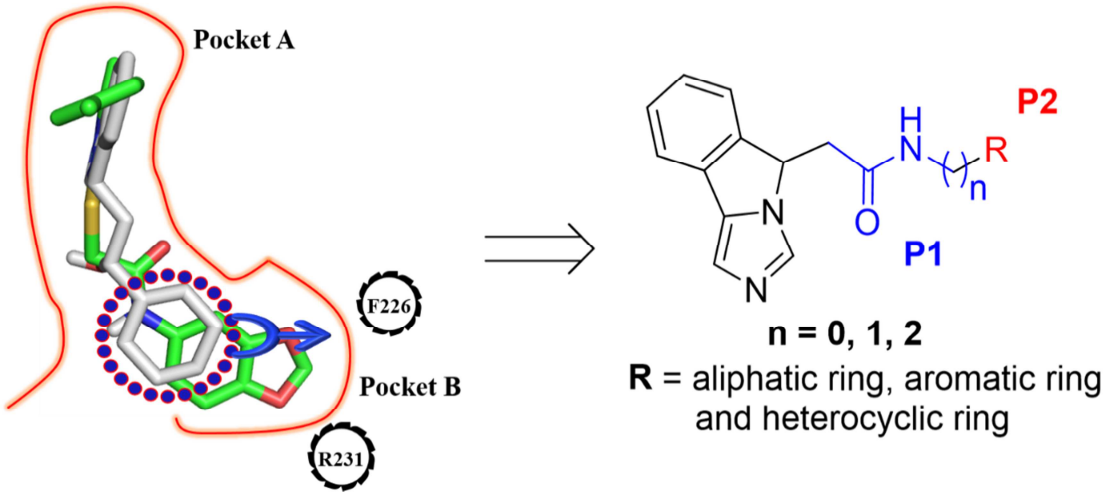

Discovery of imidazoleisoindole derivatives as potent IDO1 inhibitors: Design, synthesis, biological evaluation and computational studies

Yi Zou [a,1], Fang Wang [a,1], Yan Wang [b,1], Qirui Sun [a], Yue Hu[b], Yuezhen Li [c], Wen Liu [b], Wenjie Guo [b,*], Zhangjian Huang [a], Yihua Zhang [a], Qiang Xu [b,*], Yisheng Lai [a,**]

[a] *State Key Laboratory of Natural Medicines, Jiangsu Key Laboratory of Drug Discovery for Metabolic Diseases, Center of Drug Discovery, China Pharmaceutical University, Nanjing 210009, PR China*

[b] *State Key Laboratory of Pharmaceutical Biotechnology, School of Life Sciences, Nanjing University, Nanjing 210093, PR China*

[c] *Department of Organic Chemistry, School of Science, China Pharmaceutical University, Nanjing 211198, PR China*

Author Contributions

[1] Y.Z., F.W. and Y.W. contributed equally to this work.

[*] Corresponding author. State Key Laboratory of Pharmaceutical Biotechnology, School of Life Sciences, Nanjing University, Nanjing 210093, PR China.

[**] Corresponding author. State Key Laboratory of Natural Medicines, Jiangsu Key Laboratory of Drug Discovery for Metabolic Diseases, Center of Drug Discovery, China Pharmaceutical University, Nanjing 210009, PR China.

E-mail addresses: guowj@nju.edu.cn (W. Guo), molpharm@163.com (Q. Xu), yslai@cpu.edu.cn (Y. Lai).

ABSTRACT

Indoleamine-2,3-dioxygenase-1 (IDO1) is an attractive target for cancer immunotherapy. Herein, a series of novel imidazoleisoindole derivatives was prepared and evaluated for their ability to inhibit IDO1. Among these, derivative **11r** was the most active compound with nanomolar potency in the Hela cell-based assay, while showed negligible cellular toxicity. UV-visible spectra study demonstrated that compounds **11p** and **11r** bound to IDO1 and coordinated with the heme iron. Furthermore, they could significantly promote T cell proliferation, increase IFN-γ production, and reduce the numbers of $Foxp3^+$ regulatory T cells. Finally, induced fit docking (IFD) and quantum mechanics/molecular mechanics (QM/MM) calculation were performed to understand the interactions of these compounds to IDO1 protein, which provided a comprehensive guide for further structural modification and optimization.

Keywords:

Indoleamine 2,3-dioxygenase 1; Imidazoleisoindole; Induced fit docking; QM/MM calculation

1. Introduction

Immune escape is a fundamental trait of cancer growth and progression, and also a significant barrier to clinical immunotherapy for cancer [1,2]. Growing evidence indicates that the dysregulation of the kynurenine pathway of tryptophan metabolism is one of the key molecular mechanisms that enables tumor cells to thwart the host immune response [3,4]. The cytosolic enzyme indoleamine 2,3-dioxygenase 1 (IDO1) is the most broadly expressed "gatekeeper" enzyme that catalyzes the rapid degradation of tryptophan in the initial step of the kynurenine pathway. Nonetheless, the overexpression of IDO1 by a wide variety of tumor cells and antigen presenting cells has been observed in the tumor microenvironment [5]. The resulting local depletion of tryptophan causes cell cycle arrest of T lymphocytes and makes these cells more sensitive to apoptosis by activating the amino acid-sensitive general control non-derepressible 2 (GCN2) stress kinase pathway [6,7], and the accumulating kynurenine as well as its downstream metabolites can induce the differentiation of naïve $CD4^+$ T cells into immunosuppressive regulatory T cells (Tregs) by binding to the aryl hydrocarbon receptor (AHR) [8,9]. Similar to other immune checkpoints, IDO1 is therefore suggested to be an important target for immunotherapeutic intervention [10].

In the past decade, many small molecular IDO1 inhibitors have been identified from natural products [11-13], high-throughput screening [14-16], and structure-based design [17-19]. However, most of them either showed low potency or failed in vivo assay, so developing IDO1 inhibitors is still challenging [20,21]. To the best of our knowledge, there is no drug approved as IDO1 inhibitor until now, and only a few of small molecule IDO1 inhibitors entered clinical trials as a strategy for the treatment of cancer (*e.g.*, indoximod, epacadostat and GDC-0919) (Fig. 1) [22]. Consequently, the discovery of a novel and potent IDO1 inhibitor, which might be safe and efficacious in further development stages, remains necessary.

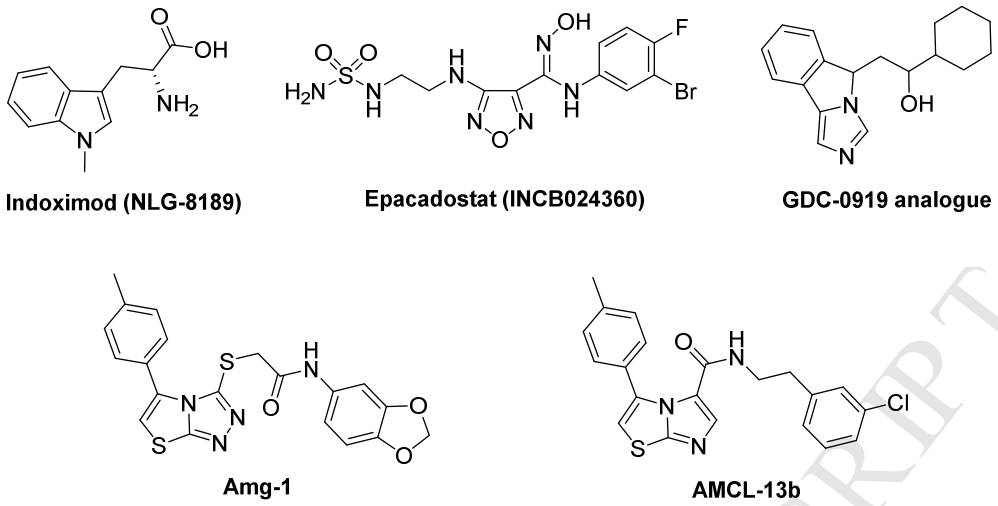

Fig. 1. The representative IDO1 inhibitors.

GDC-0919 (formerly known as NLG919, structure not disclosed), developed by NewLink Genetics and later licensed to Genentech in 2014, is a potent and orally available IDO1 inhibitor with values of *K*i = 7.2 nM and EC_{50} = 75 nM in cell-free assays [23]. Preclinical studies demonstrated that GDC-0919 displayed a favorable pharmacologic and toxicity profile, and showed significant T cell activation and antitumor activity alone and in combination with chemotherapeutics or other checkpoint inhibitors in solid tumor models [23,24]. The safety and preliminary efficacy of GDC-0919 employed as a standalone therapeutic intervention and combination treatment with anti-PD-L1 antibody atezolizumab are recently being assessed in patients with locally advanced or metastatic solid tumors [25].

More recently, Wu and co-workers published a crystal structure of IDO1 bound to a GDC-0919 analogue (PDB ID: 5EK3), which revealed that the imidazole nitrogen atom of the compound coordinated with the heme iron, and the imidazoleisoindole core was deeply placed into pocket A, while the 1-cyclohexylethanol moiety was extended towards pocket B [26]. The hydroxyl group concurrently interacted with the 7-propionic acid of the heme by an intermolecular hydrogen bond and the isoindole nitrogen by an intramolecular hydrogen bond, which was found to be crucial to inhibit IDO1. Meanwhile, the authors minimally modified the imidazoleisoindole core by other bioisosteric groups that resulted in the dramatic loss of IDO1 inhibitory activity, which indicated the

importance of this moiety for the inhibition of IDO1.

Through meticulous observation of the active site of this IDO1/ GDC-0919 analogue co-crystal, it is found that the 1-cyclohexylethanol moiety stretches itself to the entrance of the pocket B, not fully occupying it (Fig. 2). That's mainly because the hydrogen bonding network appears between the inhibitor and IDO1 protein that could control the conformation of the molecules [27, 28]. Tojo *et al.* from Dainippon Sumitomo Pharma Co. pointed out the generation of an induced fit and the resulting interaction with Phe226 and Arg231 in pocket B were essential for potent IDO1 inhibitory activity through the crystallization of IDO1/Amg-1 and IDO1/AMCL-13b complexes [29]. These results provide new directions for developing novel IDO1 inhibitors that simultaneously occupy pocket A and B.

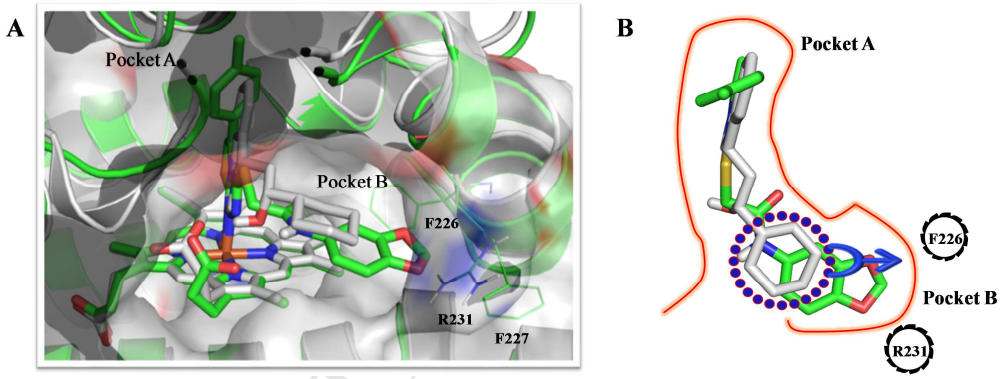

Fig. 2. (A) The superposition of the active site of two IDO1 co-crystals. PDB ID: 4PK5 (colored in green), 5EK3 (colored in grey). (B) Top view of two aligned ligands. Amg-1 is colored in green, and GDC-0919 analogue is colored in grey. The red curve represents the shape of the binding pocket.

Therefore, for continuously identifying potent IDO1 inhibitors [30,31], in this study, we reported the extensive structural modification of GDC-0919 analogue. Given that the imidazoleisoindole core is a very important heterocyclic scaffold for IDO1 binding in the structure of GDC-0919 analogue [32-34], we decided to take advantage of this skeleton as a privileged scaffold and modify it on site P1 by using different linker length and flexibility and site P2 by different substituted aromatic and aliphatic ring (Fig. 3), thereby designing a new series of imidazoleisoindole derivatives. Interestingly, the resulting compounds **11p** and **11r** proved to be potent inhibitors of IDO1 with no/negligible

cytotoxicity. Subsequent experiments indicated that these compounds could promote T cell proliferation, increase IFN-γ production, and reduce the conversion of naïve T cells into Tregs. Furthermore, the binding mode analysis of them based on induced fit docking (IFD) and quantum mechanics/molecular mechanics (QM/MM) calculation will give us a direction for further structure optimization.

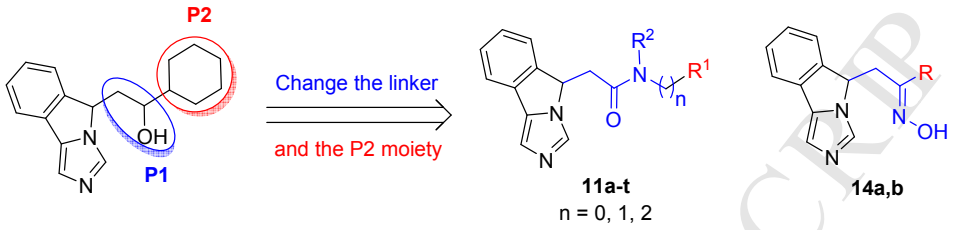

Fig. 3. Design strategy for novel imidazoleisoindole derivatives.

2. Results and discussion

2.1. Chemistry

Synthetic route for the target compounds **11a-t** was shown in scheme 1. 4,5-Diiodo-1*H*-imidazole **2** was prepared from 1*H*-imidazole and iodine, and followed by refluxing in ethanol in the presence of sodium sulfite to afford 4-iodo-1*H*-imidazole **3**. The resulting compound was subsequently protected with triphenylmethyl chloride to yield **4**, which was then converted into the key benzaldehyde **6** by Suzuki cross-coupling reaction with phenylboronic acid **5**. Ethyl acrylate **8** was obtained by Wittig reaction of **6** with the reagent **7**, and then cyclized by an intramolecular Michael reaction in refluxing acetic acid to prepare imidazoleisoindole **9**. The acetic acid **10** was obtained from **9** by hydrolysis reaction, followed by esterification with various aromatic amines in the presence of 1-hydroxybenzotriazole (HOBT) and *N*-ethyl-*N*′-(3-dimethylaminopropyl) carbodiimide (EDCI) to form compounds **11a-t**.

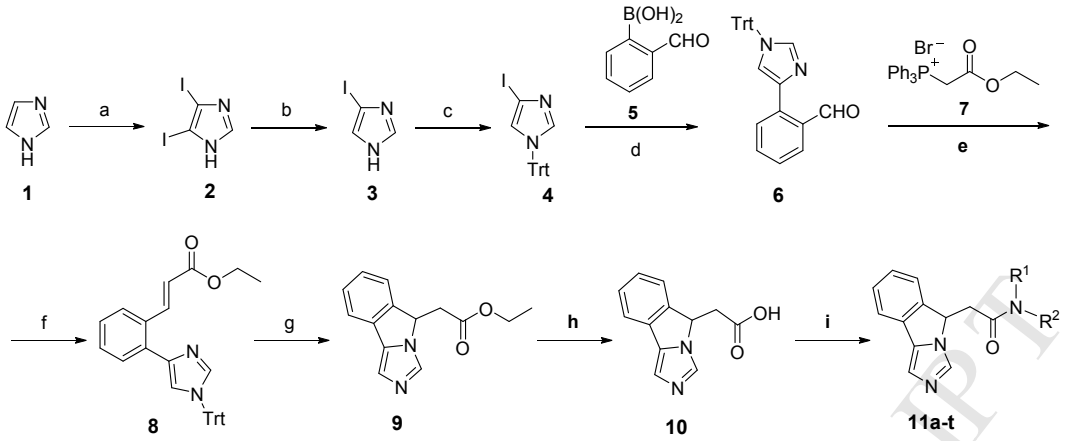

Scheme 1. Reagents and conditions: (a) NaOH, I_2, KI, H_2O, 20 ^oC, 1 h, 99.0%; (b) Na_2SO_3, EtOH, reflux, 24 h, 48.1%; (c) TrtCl, TEA, DMF, 20 ^oC, 48 h, 94.0%; (d) $Pd(PPh_3)_4$, K_3PO_4, DMF, H_2O, N_2, 90 ^oC, 66.7%; (e) PPh_3, DCM, rt, 90.6%; (f) NaOH, H_2O, DCM, rt, 77.5%; (g) HOAc, MeOH, reflux, 3 h, 76.0%; (h) NaOH, EtOH, H_2O, 60 ^oC; (i) EDCI, HOBT, TEA, DMF, rt.

Synthetic route for the target compounds **14a** and **14b** was shown in scheme 2. The direct aldol reaction was applied to **6** to give key intermediates **12a** and **12b**, which were cyclized in refluxing acetic acid to afford imidazoleisoindoles **13a** and **13b**. Subsequent condensation of hydroxylamine hydrochloride with **13a** and **13b** to yield compounds **14a** and **14b**.

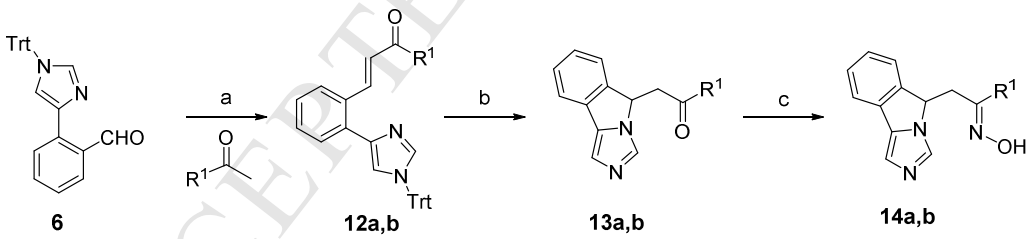

Scheme 2. Reagents and conditions: (a) Na, EtOH, rt, 3 h; (b) HOAc, MeOH, reflux, 3 h; (c) $NH_2OH \cdot HCl$, EtOH, 50 ^oC, 12 h.

2.2. Inhibition of IDO1 activity in a cell-based assay

It is well-known that IDO1 enzymatic and cellular assays have greater biological relevance and reported correlation issues [35]. Thus, HeLa cell line expressing native human IDO1 induced with IFN-γ was chosen as the primary screen for investigating the therapeutic potential of the newly synthesized compounds. This cellular assay is beneficial

to drug development, as it not only evaluates the IDO1 inhibitory activity of the tested compounds, but also measures their cytotoxicity on cell, and predicts their permeability [11,15]. Both GDC-0919 analogue (GDC-0919 racemic mixture) and *L*-1-MT were used as positive controls.

As shown in Table 1, we first investigated compounds **11a-11m** with the linker having four heavy atoms that may facilitate the P2 moiety sticking into pocket B. Quite disappointingly, almost all compounds showed weak potency against IDO1 no matter what R^1 group was electron withdrawing (**11a-11e**, **11k-11m**) or electron donating (**11f**, **11g**, **11j**) aromatic nucleus. Meantime, **11h** and **11i**, which have a methyl group linked to amide and methylene moieties, respectively, could not improve the inhibitory activity of **11a**. However, attempts at rigidifying the linker with three heavy atoms got some positive results (**11n-11o**), which were more potent than compounds **11a-11m**. Especially, **11p** gave a 13-fold improvement in inhibitory potency compared with the counterpart **11j**, both of which contained the same 1,3-benzodioxolyl moiety towards pocket B. Following these encouraging results, we next explored compounds **11r-11t** to see if the linker with five heavy atoms could increase the potency. Surprisingly, their cell-based inhibitory activities were much better than the corresponding series with three or four atoms linker (**11r** *vs* **11f**; **11s** *vs* **11a** and **11n**; **11t** *vs* **11l**). Among them, compound **11r** was the most potent derivative in the series, which was in the same order of magnitude as GDC-0919 analogue. Finally, hydroxyl group in GDC-0919 analogue was replaced by hydroxyloxime, but leading to **14a** and **14b** which exhibited poor activity with IC_{50} values higher than 20 μM.

Furthermore, the results from **11n-11q** and **11r-11t** showed that the inhibitory activity of compounds bearing an electron-donating aromatic ring was obviously greater than that of one bearing an electron-withdrawing aromatic ring (**11p** *vs* **11o**; **11r** *vs* **11t**), while the activity of the latter was weaker than the corresponding benzene without substituent (**11o** *vs* **11n**; **11t** *vs* **11s**). At first glance, these results appear to be contradictory about the correlation between the activity and the linker length of compounds (**11a**, **11n** and **11s**). The discussion about this will be performed in the next section. Among these compounds, **11p** and **11r** were the two most active derivatives with IC_{50} values of 5.03 μM and 0.84

μM, respectively, which were selected for further evaluation.

Table 1. Structures of the target compounds and their activity for inhibiting IDO1.

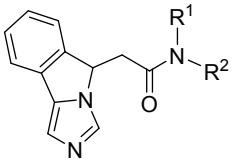

11a-t

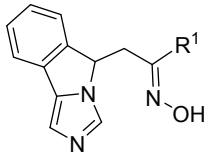

14a,b

Compd.	R^1	R^2	IC_{50} (μM)[a]	Compd.	R^1	R^2	IC_{50} (μM)[a]
11a	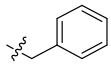	H	60.56	**11m**	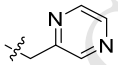	H	65.92
11b	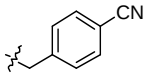	H	69.44	**11n**		H	25.93
11c	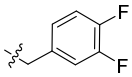	H	58.11	**11o**	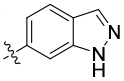	H	33.1
11d	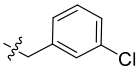	H	53.93	**11p**	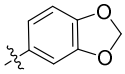	H	5.03
11e	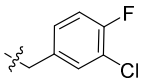	H	50.9	**11q**		H	39.04
11f	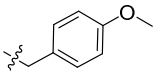	H	77.54	**11r**	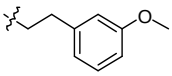	H	0.84
11g	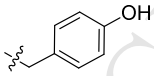	H	71.7	**11s**	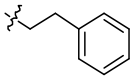	H	14.98
11h	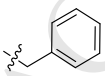	CH_3	64.47	**11t**	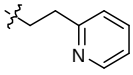	H	21.93
11i	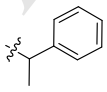	H	74.39	**14a**			20.37
11j	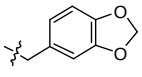	H	66.73	**14b**	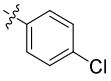		22.72

11k	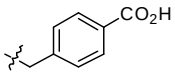	H	95.07	***L*-1-MT**	14.69
11l	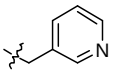	H	82.12	**GDC0919**[b]	0.26

[a] Results are mean of at least two experiments. [b] GDC-0919 analogue [26]

*2.3. Effects of **11p**, **11r** and **11s** on cell viability*

Since the inhibition of tryptophan degradation could simply be an effect of the cytotoxicity of the tested compounds, measurement of cell viability is indispensable when reporting cellular IC_{50} values. In this study, for all compounds, the viability of Hela cells was measured with the MTT method at the end of the IDO1 cellular assay. The results of this assay indicated that most of the compounds displayed no/negligible level of toxicity under the experimental conditions. The results of cell viability assay of **11p**, **11r** and **11s** were shown in Fig. 4A.

*2.4. Effects of **11p**, **11r** and **11s** on IDO1 expression*

Since the suppression of IDO1 expression of the tested compounds could also be responsible for the inhibitions of tryptophan degradation, Western blot analysis was subsequently performed to investigate if compounds **11p**, **11r** and **11s** could affect the expression of IDO1 protein in the HeLa cell-based assay. The results showed that these three compounds didn't influence IDO1 protein level (Fig. 4B), which indicated that they inhibited IDO1 enzymatic activity and not its expression in cells. Similarly, GDC-0919 analogue also did not affect IDO1 expression in Hela cells.

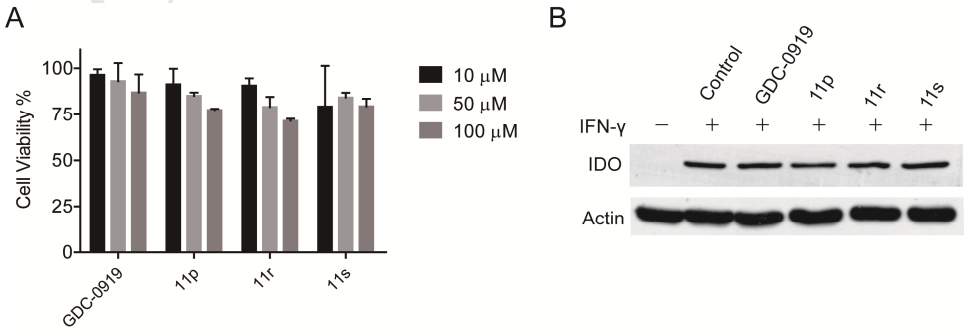

Fig. 4. (A) Measurement of cytotoxicity of compounds **11p**, **11r** and **11s**. Cell viability was determined by the MTT assay. Data are averages from at least three independent experiments. (B) HeLa cells were

treated with IFN-γ with or without compounds **11p**, **11r** and **11s** at their IC_{50} concentrations for 24 hours, and analyzed by Western blot using an anti-IDO antibody. GDC-0919 analogue was used as a reference.

*2.5. UV-visible spectra study of **11p** and **11r***

IDO1 has a heme in protein, and the specific UV absorption properties of porphyrins are useful in studies of heme-contained proteins. Since the absorbance spectra of the heme group is highly sensitive to the changes in the polarity of heme surroundings upon the ligand binding, the changes in the absorbance spectra could be utilized to evaluate the binding of the compound to IDO1 [36]. The UV−visible spectra of ferric IDO1 were measured in the presence and absence of these two compounds in this study. As can be seen from Fig.5, in the presence of compound **11p**, the Soret peak shifted from 404 to 410 nm and compound **11r** shifted the maxima from 404 to 412 nm, which indicated that these compounds bound to IDO1 and coordinated with the iron of the heme group.

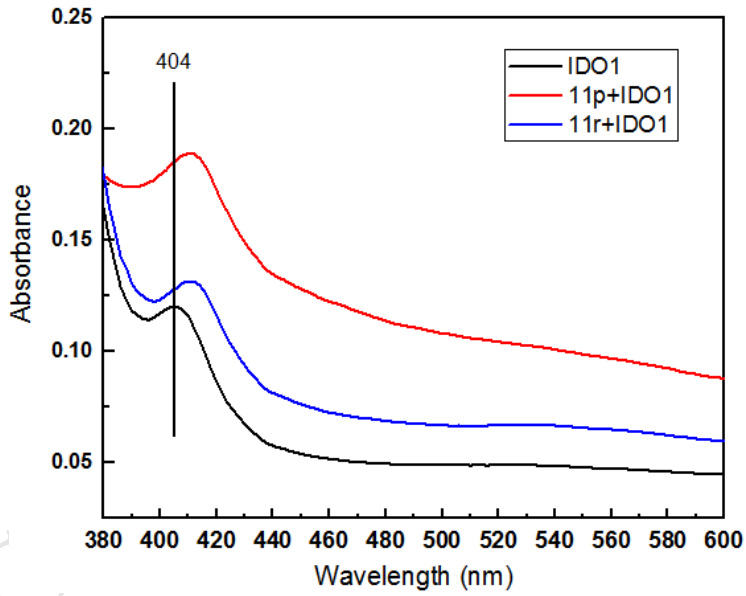

Fig. 5. UV spectra of ferric-IDO1 (black), compound **11p**-IDO1 (red) and compound **11r**-IDO1 (blue).

*2.6. Effects of **11p** and **11r** on T cell proliferation and IFN-γ production*

It is well-known that IDO1 protein is overexpressed by a variety of tumor cell types, leading to the local depletion of tryptophan levels and the production of toxic tryptophan metabolites [37]. This severely affects the proliferation of T lymphocytes and is thereby profoundly immunosuppressive [38]. A proliferation assay was carried out to determine if

inhibition of IDO1 activity could improve T cell activity in the presence of cancer cells. B16F1 cells, which expressed IDO1 in high level, were thus used to co-culture with T cells. As shown in Fig. 6A, compounds **11p**, **11r** and GDC-0919 analogue displayed a significant augmentation of T cell stimulated with B16F1 cells. Especially, compound **11p** showed 48% on the rate of T cell proliferation. These results were in conformity with the increase of IFN-γ levels compared with T cells and B16F1 co-culture system, which can increase the growth of the neighboring T cells (Fig. 6B). These findings suggested that compounds **11p** and **11r** could reverse the suppression of T lymphocytes caused by IDO1 to a great extent.

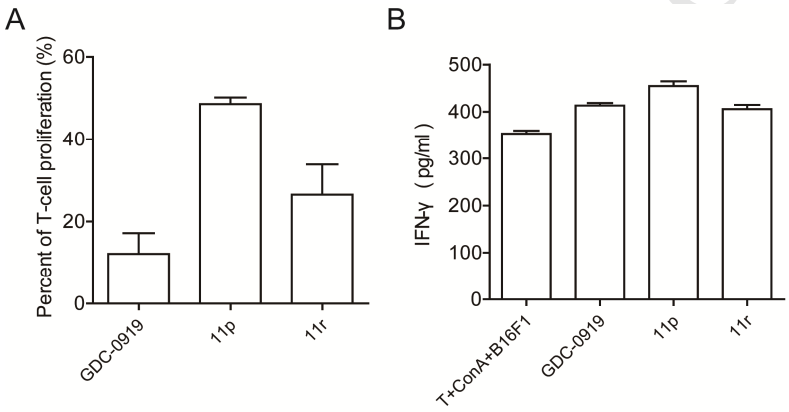

Fig. 6. T cell proliferation (A) and IFN-γ levels (B) assays in the B16F1-T cells co-culture system. Compounds **11p** and **11r** were added to the system at the concentration of their triple IC_{50} values from the HeLa-based assay (GDC-0919: 1.5 μM; **11p**: 15 μM; **11r**: 3 μM). Each bar of the graph indicates the mean of three replicate wells with standard error of the mean.

*2.7. Effects of **11p** and **11r** on Foxp3$^+$ Tregs in B16F1 cells*

It has been reported that IDO1-mediated tryptophan catabolism facilitates the conversion of naïve T lymphocytes into $CD4^+$ $CD25^+$ Tregs, which can block T cell activation and trigger T cell apoptosis, thus promotes immunoescape and favors tumor cell growth [39]. Based on these reasons, compounds **11p** and **11r** were evaluated to elucidate their effect on reversing the conversion. As shown in Fig. 7, when naïve T cells co-cultured with B16F1 cells, it gave rise to an approximately 2.7-fold increase in the number of Tregs. However, addition of **11p** and **11r** to the cultures partially reversed this effect, as did treatment with GDC-0919 analogue. These results indicated that compounds

11p and **11r** could significantly reduce the numbers of Foxp3$^+$ Tregs in B16F1 cells.

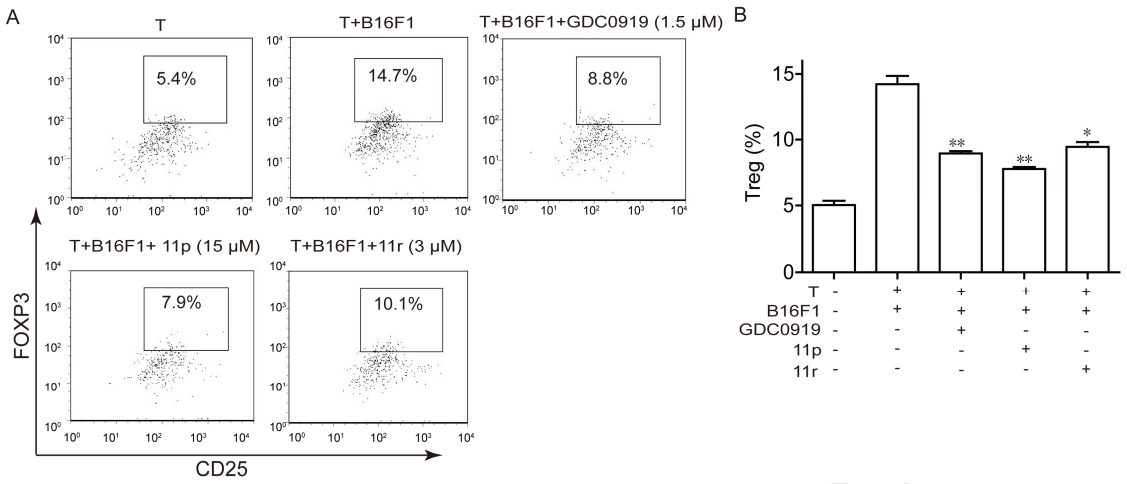

Fig. 7. Compounds **11p** and **11r** decreased differentiation of Tregs in B16F1-T cell co-culture system. (A) A representative plot of FACS analysis is presented. CD4$^+$ CD25$^+$ FOXP3$^+$ positive cells were defined as Tregs. (B) Average values of 3 independent experiments are shown in the graph. Error bars represent SD. $^*p < 0.05$, $^{**}p < 0.01$ *vs* T+B16F1.

2.8. Molecular modeling studies

Over the last decades, docking is becoming increasingly popular and has been successfully applied in several lead-compound-discovery projects [40]. Most docking algorithms rely on a rigid protein structure, which in many cases is sufficient to find some active compounds. This is often referred to as “semi-flexible docking”. However, in the case of IDO1 protein, high flexibility of side chain and backbone often poses a problem for IDO1 docking, which could lead to the formation of different active site conformations. Thus, the induced fit phenomenon should be considered here for IDO1 docking studies. In our previous studies, docking that considered the flexibility of protein was found to enhance the accuracy of predicted binding mode of IDO1 [31]. According to the induced fit theory, proteins need not be rigid locks. They can accommodate the substrate by flexibly adapting their substrate-binding site [41]. To explore the binding modes of the target compounds with the active site of IDO1, compounds **11j**, **11p** and **11r** were docked into the binding site of IDO1 by the *induced fit docking* protocol in Schrödinger. According to Wu’s research, GDC-0919 analogue contains two chiral centers and has four stereoisomers, but only two of them display high affinity against IDO1 [26]. Thus, the

absolute configuration of our chiral molecules with top rank was retained for further analysis.

In addition to the protein flexibility, the iron-ligand interaction in the active site of IDO1 is difficult to reliably describe by classical molecular force-field parameters, which could not consider the charge transfer when the ligand coordinating to the metal [42]. Quantum mechanical calculations has been shown to increase computational accuracy but it has some disadvantages including high computational cost and corresponding intractability of large chemical systems. An alternative approach is hybrid QM/MM, which was initially proposed by Warshel and Levitt in 1976 [43]. In a QM/MM simulation, a small region of the system that is of particular chemical importance was chosen to be treated using QM, while the remainder of the system is treated via MM, which offers a good balance of physical accuracy and relatively low computational cost. Based on the views mentioned above, QM/MM strategy will be performed to optimize the IDO1-inhitbitor IFD-docking complex. In our system, the QM region included the full heme ring, the iron, the coordinating His residue and the inhibitor, which maintained the complex's sixfold coordinated system, and the remaining subsystem was treated with the MM method.

As shown in Fig. 8, the overall structural features of QM/MM-optimized structures were similar to those obtained by IFD docking. The main difference included the key distance between iron atom and the corresponding coordinate atom and the orientation of the polar atoms in ligand that faced the 7-propionate group of the heme. All of imidazoleisoindole rings in the ligands were buried in hydrophobic pocket A like GDC-0919 analogue in the co-crystals (Fig. 2A). The binding modes of compound **11j** presented the similar binding conformation with Amg-1. The benzyl group connected with amide linker extended into the pocket B and its dioxomethylene oxygen formed a hydrogen bond interaction with Arg231. The NH of amide unit made a hydrogen bond with the backbone of Gly262. Unlike **11j** and **11r**, the linker length of **11p** was so short that the aniline moiety can’t stretch inside the pocket B. Nonetheless, the NH of amide linker could interact with the 7-propionate group after QM/MM optimization and the

dioxomethylene-substituted aniline ring of **11p** formed a π-cation interaction with Arg231. Although the linker length of **11j** was longer than that of **11p**, which could more stretch into pocket B, the difference of IDO1 inhibitory activity between them might be attributed to the formation of hydrogen bond interaction between the ligand and the heme 7-propionate. In the case of **11r**, the *m*-methoxyl-phenyl group was bent sharply at the methylene moiety and almost fully occupied pocket B, demonstrating the interaction with Phe226 and Arg231 through π-π and π-cation interaction, respectively. In addition to that, the amide NH in the linker was hydrogen-bonded with the heme 7-propionate like **11p**. This computational study finds that there are two dominating factors affecting IDO1 inhibitory activity: the occupation of pocket B and the resulting interaction with the 7-propionate group, which could be useful for further optimization.

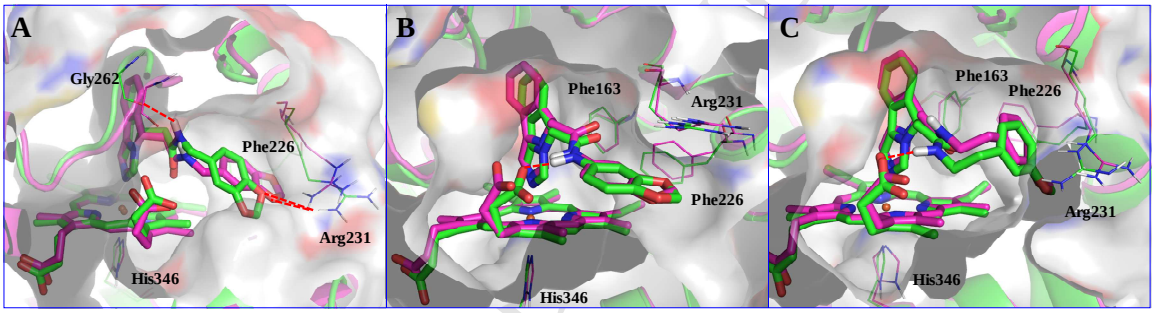

Fig. 8. The superposition of IFD-based structure (colored in magenta) and QM/MM-optimized structure (colored in green). Polar contacts were shown as red lines. (A) **11j**-IDO1 complexes, (B) **11p**-IDO1 complexes, (C) **11r**-IDO1 complexes.

3. Conclusions

IDO1 plays a key role in tryptophan catabolism in the immune system and is also considered as an important therapeutic target for the treatment of cancer and other diseases that are linked with kynurenine pathway. In this study, a series of imidazoleisoindole derivatives **11a-t** and **14a-b** were designed, synthesized and evaluated as novel IDO1 inhibitors. Structure and activity relationship analysis indicated that the compounds with three or five atoms linker showed stronger inhibitory activity than those with four atoms linker in an assay which measured IDO1 activity in cells, and the compound with an electron-donating aromatic ring at site P2 could increase inhibitory potency. Among them,

compounds **11p** and **11r** exhibited the highest inhibitory potency with no/negligible cytotoxicity. UV spectra analysis revealed that these compounds could bind to IDO1 and coordinate with the iron of the heme group. Importantly, they significantly promoted proliferation of T lymphocytes and led to the dramatic decrease of Tregs in the B16F1 and naïve T cells co-culture system. Finally, IFD and QM/MM calculation were carried out and showed that the occupation of pocket B and the resulting interaction with the 7-propionate group would be essential for potent IDO1 inhibitory activity, which could guide us for further structure optimization.

4. Experimental section

4.1. Chemistry

4.1.1. General procedures

Melting points were determined on a RDCSY-I capillary apparatus and were uncorrected. All materials used were commercially available and used as supplied. HG/T2354-92 silica gel 60 F_{254} sheets were used for analytical thin-layer chromatography (TLC). Column chromatography was performed on silica gel (200-300 mesh). ^{1}H NMR spectra were recorded on a Bruker AV-300 spectrometer. Chemical shifts (δ) were given in parts per million (ppm) relative to the solvent peak. IR spectra were recorded on shimadzu IRTracer-100 in KBr with absorptions in cm^{-1}. All the reagents and solvents were reagent grade and were used without further purification unless otherwise specified. The purity of compounds used for biological evaluations was determined to be greater than 95% using Shimadzu HPLC system (Kyoto, Japan. see Supplementary material).

*4.1.2. Preparation of intermediates **2-10***

*4.1.2.1 4,5-diiodo-1H-imidazole (**2**)*

A mixture of KI (29.3 g, 176.0 mmol) and I_2 (22.4 g, 88.0 mmol) in water (60 mL) was added to a solution of 1*H*-imidazole (3.0 g, 44.1 mmol) in 2 M NaOH (10.6 g, 264.5 mmol). The mixture was stirred at 20 °C for 3 h and then neutralized with 6 M HCl (pH = 7). The resulting solid was collected by filtration, recrystallization from ethanol to give **2** as a grey solid (14.0 g, 99.0%). Mp 166-168 °C. ^{1}H NMR (300 MHz, DMSO-d_6) δ(ppm)

12.75 (br s, 1H), 7.8 (br s, 1H). MS (EI) *m/z* 320.8 $[M+H]^+$.

*4.1.2.2 4-iodo-1H-imidazole (**3**)*

A mixture of **2** (12.0 g, 37.5 mmol) and Na_2SO_3 (23.6 g, 187.3 mmol) in EtOH (120 mL) and H_2O (20 mL) was refluxed for 72 h. The mixture was concentrated in vacuo and the residue was extracted with ethyl acetate. The crude product was purified by recrystallization from dichloromethane to afford **3** as a white solid (3.5 g, 48.1%). Mp 137-139 °C. ^{1}H NMR (300 MHz, Chloroform-*d*) δ(ppm) 7.0 (s, 1H), 7.5 (s, 1H). MS (EI) *m/z* 194.9 $[M+H]^+$.

*4.1.2.3 4-iodo-1-trityl-1H-imidazole (**4**)*

To a solution of **3** (3.5 g, 18.0 mmol) in DMF (70 mL) was added TEA (3.0 mL, 21.7 mmol) and trityl chloride (5.5 g, 19.7 mmol). After stirring at 20 °C for 24 h, the solution was poured into water. The solid was filtered to yield the crude compound that was purified by flash column chromatography on silica gel to afford **4** as a white solid (7.4 g, 94.0%). Mp 148-150 °C. ^{1}H NMR (300 MHz, Chloroform-*d*) δ(ppm) 6.9 (m, 1H), 7.0-7.2 (m, 6H), 7.25-7.4 (m, 10H). MS (EI) *m/z* 437.1 $[M+H]^+$.

*4.1.2.4 2-(1-trityl-1H-imidazol-4-yl)benzaldehyde (**6**)*

A suspension of **4** (3.0 g, 6.9 mmol), the appropriate 2-formyl boronic acid (1.6 g, 10.7 mmol) and K_3PO_4 (4.4 g, 20.8 mmol) in DMF (30 mL) and water (6 mL) was purged with nitrogen for 5 min, followed by the addition of $Pd(PPh_3)_4$ (0.6 g, 0.5 mmol) and the mixture was purged with nitrogen for another 5 mins. The reaction mixture was stirred at 90 °C for 16 h under an atmosphere of N_2. The solution was allowed to cool and was filtered through a plug of celite. The mixture was diluted with water (50 mL) and was extracted with ethyl acetate to afford the crude product which was purified by flash column chromatography on silica gel to yield **6** as a white solid (1.9 g, 66.7%). Mp 147-149 °C. ^{1}H NMR (300 MHz, Chloroform-*d*) δ(ppm) 7.97 (dd, *J* = 7.8, 1.4 Hz, 1H), 7.72-7.54 (m, 3H), 7.38 (h, *J* = 3.2 Hz, 11H), 7.25-7.19 (m, 6H), 7.07 (d, *J* = 1.3 Hz, 1H). MS (EI) *m/z* 415.2 $[M+H]^+$.

*4.1.2.5 Wittig reactant ethyl 2-(triphenyl-λ^5-phosphanylidene)acetate (**7**)*

The solution of triphenylphosphane (25.9 g, 98.8 mmol) in dichloromethane (300 mL) was added ethyl 2-bromoacetate (15.0 g, 89.8 mmol) dropwise, and stirred at room temperature for 3 days. After the evaporation of the solvent, the remaining residue was collected and washed with dichloromethane three times to give the corresponding Wittig reactant as a white solid (35.0 g, 90.6%).

*4.1.2.6 An optical mixture of ethyl (Z)-3-(2-(1-trityl-1H-imidazol-4-yl)phenyl)acrylate and ethyl (E)-3-(2-(1-trityl-1H-imidazol-4-yl)phenyl)acrylate (**8**)*

To a suspension of NaOH (0.6 g, 15.4 mmol) in water (1 mL) at 0 °C was added 7 (3.3 g, 7.7 mmol) as a solution in dichloromethane (10 mL) and the mixture was stirred for 40 min. The intermediate **6** (3.2 g, 7.7 mmol) was added as a solution in dichloromethane (10 mL) drop wise over a period of 3 min. The reaction was allowed to room temperature and stirred overnight. The mixture was diluted with water and was extracted with dichloromethane to afford the crude product which was purified by flash column chromatography on silica gel to yield **8** as a faint yellow solid (2.9 g, 77.5%). Mp 110-112 °C. ^{1}H NMR (300 MHz, Chloroform-*d*) δ(ppm) 8.17 (d, *J* = 15.9 Hz, 1H), 7.77 (dd, *J* = 7.8, 1.4 Hz, 1H), 7.61-7.51 (m, 3H), 7.45-7.33 (m, 14H), 7.21 (td, *J* = 7.2, 6.6, 4.1 Hz, 8H), 7.06-6.89 (m, 2H), 6.32 (d, *J* = 15.9 Hz, 1H), 4.23 (q, *J* = 7.1 Hz, 2H), 4.07 (q, *J* = 7.1 Hz, 1H), 1.29-1.24 (m, 3H), 1.15 (t, *J* = 7.1 Hz, 1H). MS (EI) *m/z* 485.3 $[M+H]^+$.

*4.1.2.7 ethyl 2-(5H-imidazo[5,1-a]isoindol-5-yl)acetate (**9**)*

To a solution of **8** (5.0 g, 10.3 mmol) in methyl alcohol (50 mL) was added AcOH (12.5 mL) and the mixture was stirred at 90 °C for 3 h. The mixture was allowed to cool to room temperature and the pH was adjusted to 10 with saturated K_2CO_3 solution. The mixture was evaporated in vacuo to remove methyl alcohol and was extracted with ethyl acetate to afford the crude product which was purified by flash column chromatography on silica gel to yield **9** as a grey solid (1.9 g, 76.0%). Mp 87-89 °C. ^{1}H NMR (300 MHz, Chloroform-*d*) δ(ppm) 7.81 (s, 1H), 7.57 (dt, *J* = 7.6, 1.0 Hz, 1H), 7.49-7.42 (m, 2H), 7.35 (dd, *J* = 1.7, 1.0 Hz, 1H), 7.21 (s, 1H), 5.58 (s, 1H), 4.30 (q, *J* = 7.1 Hz, 2H), 3.12 (dd, *J* = 17.3, 3.9 Hz, 1H), 2.73 (dd, *J* = 17.3, 9.7 Hz, 1H), 1.33 (t, *J* = 7.2 Hz, 3H). MS (EI) *m/z* 243.1 $[M+H]^+$.

*4.1.2.8 2-(5H-imidazo[5,1-a]isoindol-5-yl)acetic acid (**10**)*

To a solution of **9** (1.0 g, 4.1 mmol) in ethyl alcohol (50 mL) was added NaOH (0.8 g, 20.6 mmol) in water (2 mL) and the mixture was stirred at 60 °C for 3 h. After the reaction mixture was allowed to cool to room temperature, the pH was adjusted to 5-6 with 10% hydrochloric acid. Then, the mixture was evaporated in vacuo to remove solvent to afford the crude product **10**, which was used to the next step without any purification; MS (EI) *m/z* 215.1 $[M+H]^+$.

*4.1.3. General preparation of compounds **11a-t***

To the crude product **10** (1 mol equiv) in DMF (0.12 M) was added EDC (1.2 mol equiv), HOBT (1.2 mol equiv) and TEA (3 mol equiv) and the mixture was stirred at room temperature for 15 min. After that, the mixture was added various aromatic or aliphatic amines (1.1 mol equiv), then it was stirred at room temperature for 12 h. The mixture was diluted with water and was extracted with ethyl acetate to afford the crude product which was purified by flash column chromatography on silica gel to yield the target products.

*4.1.3.1. N-benzyl-2-(5H-imidazo[5,1-a]isoindol-5-yl)acetamide (**11a**)*

Yield 67.2%. White powder. Mp 140-142 °C. ^{1}H NMR (300 MHz, Chloroform-*d*) δ(ppm) 7.61 (s, 1H), 7.51 (d, *J* = 7.5 Hz, 1H), 7.43-7.32 (m, 7H), 7.24 (d, *J* = 8.1 Hz, 1H), 7.08 (s, 1H), 6.55 (s, 1H), 5.67 (dd, *J* = 9.4, 4.5 Hz, 1H), 4.62-4.40 (m, 2H), 2.94 (dd, *J* = 15.4, 4.4 Hz, 1H), 2.50 (dd, *J* = 15.4, 9.5 Hz, 1H). MS (EI) *m/z* 304.2 $[M+H]^+$. IR (KBr) 3207, 3030, 1652, 1615, 1504 cm^{-1}.

*4.1.3.2. N-(4-cyanobenzyl)-2-(5H-imidazo[5,1-a]isoindol-5-yl)acetamide (**11b**)*

Yield 60.4%. Pale yellow powder. Mp 198-200 °C. ^{1}H NMR (300 MHz, DMSO-d_6) δ(ppm) 8.70 (t, *J* = 5.9 Hz, 1H), 7.87-7.74 (m, 2H), 7.69-7.52 (m, 2H), 7.5-7.33 (m, 4H), 7.26 (td, *J* = 7.6, 1.2 Hz, 1H), 7.13 (s, 1H), 5.62 (dd, *J* = 8.7, 5.2 Hz, 1H), 4.60-4.37 (m, 2H), 3.07 (dd, *J* = 15.4, 5.2 Hz, 1H), 2.69 (dd, *J* = 15.5, 8.8 Hz, 1H). MS (EI) *m/z* 329.1 $[M+H]^+$. IR (KBr) 3208, 3007, 2226, 1652, 1606, 1506 cm^{-1}.

*4.1.3.3. N-(3,4-difluorobenzyl)-2-(5H-imidazo[5,1-a]isoindol-5-yl)acetamide (**11c**)*

Yield 78.0%. Pale yellow powder. Mp 88-90 °C. ^{1}H NMR (300 MHz, Chloroform-*d*)

δ(ppm) 7.60 (s, 1H), 7.51 (d, *J* = 7.6 Hz, 1H), 7.36 (dd, *J* = 21.6, 7.5 Hz, 2H), 7.24 (t, *J* = 7.7 Hz, 1H), 7.19-6.97 (m, 4H), 6.91 (s, 1H), 5.66 (dd, *J* = 9.2, 4.5 Hz, 1H), 4.53 (dd, *J* = 14.9, 5.9 Hz, 1H), 4.37 (dd, *J* = 14.9, 5.4 Hz, 1H), 2.96 (dd, *J* = 15.9, 4.2 Hz, 1H), 2.56 (dd, *J* = 15.5, 9.2 Hz, 1H). MS (EI) *m/z* 340.1 $[M+H]^+$. IR (KBr) 3207, 3022, 1645, 1609, 1520 cm^{-1}.

*4.1.3.4. N-(3-chlorobenzyl)-2-(5H-imidazo[5,1-a]isoindol-5-yl)acetamide (**11d**)*

Yield 66.0%. White powder. Mp 73-75 °C. ^{1}H NMR (300 MHz, Chloroform-*d*) δ(ppm) 7.65 (s, 1H), 7.53 (d, *J* = 7.6 Hz, 1H), 7.44-7.29 (m, 4H), 7.29-7.16 (m, 3H), 7.12 (d, *J* = 1.7 Hz, 1H), 6.33 (s, 1H), 5.71 (dd, *J* = 9.4, 4.5 Hz, 1H), 4.59 (dd, *J* = 14.6, 5.8 Hz, 1H), 4.43 (dd, *J* = 15.0, 5.0 Hz, 1H), 3.08-2.86 (m, 1H), 2.66-2.41 (m, 1H). MS (EI) *m/z* 338.1 $[M+H]^+$. IR (KBr) 3213, 3024, 1645, 1599, 1472 cm^{-1}.

*4.1.3.5. N-(3-chloro-4-fluorobenzyl)-2-(5H-imidazo[5,1-a]isoindol-5-yl)acetamide (**11e**)*

Yield 67.2%. White powder. Mp 143-145 °C. ^{1}H NMR (300 MHz, Chloroform-*d*) δ(ppm) 7.67 (s, 1H), 7.54 (d, *J* = 7.6 Hz, 1H), 7.37 (dt, *J* = 14.1, 7.3 Hz, 2H), 7.30-7.22 (m, 2H), 7.14 (q, *J* = 8.2, 7.3 Hz, 2H), 6.29 (s, 1H), 5.79-5.63 (m, 1H), 4.54 (d, *J* = 5.9 Hz, 1H), 4.41 (d, *J* = 4.9 Hz, 1H), 2.99 (dd, *J* = 15.3, 4.5 Hz, 1H), 2.58 (dd, *J* = 15.4, 9.1 Hz, 1H). MS (EI) *m/z* 356.1 $[M+H]^+$. IR (KBr) 3208, 3107, 1646, 1614, 1504 cm^{-1}.

*4.1.3.6. 2-(5H-imidazo[5,1-a]isoindol-5-yl)-N-(4-methoxybenzyl)acetamide (**11f**)*

Yield 72.3%. White powder. Mp 74-76 °C. ^{1}H NMR (300 MHz, DMSO-d_6) δ(ppm) 8.52 (s, 1H), 7.77-7.55 (m, 2H), 7.47 (d, *J* = 7.6 Hz, 1H), 7.39 (t, *J* = 7.5 Hz, 1H), 7.32-7.18 (m, 3H), 7.13 (s, 1H), 6.97-6.84 (m, 2H), 5.62 (dd, *J* = 8.9, 5.2 Hz, 1H), 4.31 (d, *J* = 5.8 Hz, 2H), 3.74 (s, 3H), 3.01 (dd, *J* = 15.3, 5.3 Hz, 1H), 2.61 (dd, *J* = 15.3, 9.0 Hz, 1H). MS (EI) *m/z* 334.2 $[M+H]^+$. IR (KBr) 3275, 3050, 1651, 1612, 1512, 1248 cm^{-1}.

*4.1.3.7. N-(4-hydroxybenzyl)-2-(5H-imidazo[5,1-a]isoindol-5-yl)acetamide (**11g**)*

Yield 65.8%. White powder. Mp 232-234 °C. ^{1}H NMR (300 MHz, DMSO-d_6) δ(ppm) 9.33 (d, *J* = 1.2 Hz, 1H), 8.46 (s, 1H), 7.70-7.55 (m, 2H), 7.47 (d, *J* = 7.6 Hz, 1H), 7.39 (t, *J* = 7.4 Hz, 1H), 7.26 (dd, *J* = 7.5, 1.2 Hz, 1H), 7.17-7.01 (m, 3H), 6.79-6.63 (m, 2H), 5.62 (dd, *J* = 9.0, 5.2 Hz, 1H), 4.26 (d, *J* = 5.7 Hz, 2H), 3.00 (dd, *J* = 15.2, 5.3 Hz, 1H),

2.74-2.56 (m, 1H). MS (EI) *m/z* 320.2 $[M+H]^+$. IR (KBr) 3649, 3300, 3032, 1630, 1595, 1507, 1240 cm^{-1}.

*4.1.3.8. N-benzyl-2-(5H-imidazo[5,1-a]isoindol-5-yl)-N-methylacetamide (**11h**)*

Yield 69.1%. White powder. Mp 208-210 °C. ^1H NMR (300 MHz, Chloroform-*d*) δ(ppm) 7.86 (d, *J* = 3.5 Hz, 1H), 7.66-6.99 (m, 10H), 5.79 (d, *J* = 9.3 Hz, 1H), 4.81-4.62 (m, 1H), 4.45 (s, 1H), 3.22-3.01 (m, 2H), 2.86 (s, 3H). MS (EI) *m/z* 318.2 $[M+H]^+$. IR (KBr) 3032, 2953, 2853, 1636, 1595, 1508 cm^{-1}.

*4.1.3.9. 2-(5H-imidazo[5,1-a]isoindol-5-yl)-N-(1-phenylethyl)acetamide (**11i**)*

Yield 60.2%. White powder. Mp 144-146 °C. ^1H NMR (300 MHz, Chloroform-*d*) δ(ppm) 8.68-8.39 (d, *J* = 7.9 Hz, 1H), 7.86-7.44 (m, 3H), 7.44-7.27 (m, 6H), 7.27-7.07 (m, 2H), 5.76-5.47 (t, *J* = 7.1 Hz, 1H), 5.17-4.95 (m, 1H), 3.11-2.91 (td, *J* = 15.7, 5.3 Hz, 1H), 2.74-2.58 (dt, *J* = 16.1, 8.3 Hz, 1H), 1.47-1.34 (m, 3H). MS (EI) *m/z* 318.2 $[M+H]^+$. IR (KBr) 3273, 3030, 2966, 2853, 1645, 1622, 1520 cm^{-1}.

4.1.3.10.

*N-(benzo[d][1,3]dioxol-5-ylmethyl)-2-(5H-imidazo[5,1-a]isoindol-5-yl)acetamide (**11j**)*

Yield 74.3%. White powder. Mp 88-90 °C. ^1H NMR (300 MHz, DMSO-d_6) δ(ppm) 7.76-7.64 (s, 1H), 7.57-7.41 (m, 2H), 7.37-7.11 (m, 6H), 7.08-7.01 (d, *J* = 6.7 Hz, 1H), 5.67-5.46 (m, 1H), 4.67-4.39 (d, *J* = 2.0 Hz, 2H), 3.34-3.26 (d, *J* = 4.0 Hz, 1H), 2.87-2.75 (d, *J* = 11.1 Hz, 3H). MS (EI) *m/z* 348.1 $[M+H]^+$. IR (KBr) 3275, 3032, 1636, 1609, 1489, 1250 cm^{-1}.

*4.1.3.11. 4-((2-(5H-imidazo[5,1-a]isoindol-5-yl)acetamido)methyl)benzoic acid (**11k**)*

Yield 79.2%. White powder. Mp 260-262 °C. ^1H NMR (300 MHz, DMSO-d_6) δ(ppm) 12.84 (s, 2H), 8.68 (s, 1H), 8.03-7.81 (m, 2H), 7.72-7.53 (m, 2H), 7.49 (d, *J* = 7.4 Hz, 1H), 7.39 (d, *J* = 7.5 Hz, 2H), 7.25 (t, *J* = 7.7 Hz, 1H), 7.13 (d, *J* = 2.3 Hz, 1H), 5.62 (d, *J* = 6.6 Hz, 1H), 4.45 (s, 2H), 3.07 (dd, *J* = 15.2, 5.3 Hz, 1H), 2.68 (dd, *J* = 15.5, 8.9 Hz, 1H). MS (EI) *m/z* 348.1 $[M+H]^+$. IR (KBr) 3065, 2920, 1653, 1616, 1508, 949 cm^{-1}.

*4.1.3.12. 2-(5H-imidazo[5,1-a]isoindol-5-yl)-N-(pyridin-3-ylmethyl)acetamide (**11l**)*

Yield 59.1%. White powder. Mp 119-121 °C. ^1H NMR (300 MHz, Chloroform-*d*)

δ(ppm) 8.56-8.44 (m, 1H), 7.86 (d, *J* = 42.9 Hz, 1H), 7.68 (d, *J* = 8.0 Hz, 1H), 7.54 (d, *J* = 7.5 Hz, 1H), 7.46-7.23 (m, 5H), 7.14 (s, 2H), 5.75 (dd, *J* = 9.0, 4.4 Hz, 1H), 4.52 (dd, *J* = 20.6, 5.7 Hz, 2H), 3.09 (dd, *J* = 15.7, 4.8 Hz, 1H), 2.66 (s, 1H). MS (EI) *m/z* 305.1 $[M+H]^+$. IR (KBr) 3275, 3065, 1653, 1595, 1508 cm^{-1}.

*4.1.3.13. 2-(5H-imidazo[5,1-a]isoindol-5-yl)-N-(pyrazin-2-ylmethyl)acetamide (**11m**)*

Yield 64.1%. White powder. Mp 163-165 °C. ^{1}H NMR (300 MHz, Chloroform-*d*) δ(ppm) 8.65 (d, *J* = 4.1 Hz, 1H), 8.57-8.45 (m, 2H), 7.72 (s, 1H), 7.54 (d, *J* = 8.0 Hz, 1H), 7.38 (dd, *J* = 15.2, 7.7 Hz, 2H), 7.26 (dd, *J* = 11.4, 5.0 Hz, 1H), 7.13 (d, *J* = 4.4 Hz, 1H), 7.04 (s, 1H), 5.84-5.54 (m, 1H), 4.72 (t, *J* = 4.9 Hz, 2H), 3.13-2.95 (m, 1H), 2.63 (dd, *J* = 15.5, 9.7 Hz, 1H). MS (EI) *m/z* 306.1 $[M+H]^+$. IR (KBr) 3273, 3033, 1684, 1593, 1506 cm^{-1}.

*4.1.3.14. 2-(5H-imidazo[5,1-a]isoindol-5-yl)-N-phenylacetamide (**11n**)*

Yield 77.1%. Pale yellow powder. Mp 227-229 °C. ^{1}H NMR (300 MHz, Chloroform-*d*) δ(ppm) 7.95 (s, 1H), 7.74 (s, 1H), 7.56 (t, *J* = 7.9 Hz, 2H), 7.47-7.30 (m, 4H), 7.28 (d, *J* = 2.6 Hz, 2H), 7.17 (dd, *J* = 15.5, 7.7 Hz, 2H), 5.90-5.64 (m, 1H), 3.13 (d, *J* = 15.3 Hz, 1H), 2.73 (dd, *J* = 15.5, 9.5 Hz, 1H). MS (EI) *m/z* 290.2 $[M+H]^+$. IR (KBr) 3273, 3030, 1653, 1601, 1506 cm^{-1}.

*4.1.3.15. 2-(5H-imidazo[5,1-a]isoindol-5-yl)-N-(1H-indazol-6-yl)acetamide (**11o**)*

Yield 68.3%. White powder. Mp 280-282 °C. ^{1}H NMR (300 MHz, DMSO-d_6) δ(ppm) 8.23 (s, 1H), 7.99 (s, 1H), 7.67 (dd, *J* = 14.8, 8.3 Hz, 2H), 7.57 (d, *J* = 7.4 Hz, 1H), 7.40 (d, *J* = 7.3 Hz, 1H), 7.31 (d, *J* = 7.5 Hz, 1H), 7.20-7.02 (m, 2H), 5.73 (s, 1H), 2.89 (dd, *J* = 16.0, 9.2 Hz, 1H). MS (EI) *m/z* 330.2 $[M+H]^+$. IR (KBr) 3273, 3196, 3030, 1653, 1595, 1506 cm^{-1}.

*4.1.3.16. N-(benzo[d][1,3]dioxol-5-yl)-2-(5H-imidazo[5,1-a]isoindol-5-yl)acetamide (**11p**)*

Yield 65.9%. White powder. Mp 210-212 °C. ^{1}H NMR (300 MHz, DMSO-d_6) δ(ppm) 8.64-8.46 (t, *J* = 5.9 Hz, 1H), 7.63-7.56 (s, 1H), 7.56-7.48 (d, *J* = 7.5 Hz, 1H), 7.43-7.34 (d, *J* = 7.6 Hz, 1H), 7.33-7.23 (m, 3H), 7.21-7.11 (ddd, *J* = 7.5, 6.4, 1.4 Hz, 2H), 7.09-6.99 (s,

1H), 5.79-5.41 (dd, *J* = 8.8, 5.4 Hz, 1H), 4.50-4.09 (m, 2H), 3.07-2.87 (dd, *J* = 15.4, 5.4 Hz, 1H), 2.74-2.54 (dd, *J* = 15.4, 8.8 Hz, 1H). MS (EI) *m/z* 334.1 $[M+H]^+$. IR (KBr) 3275, 3078, 1636, 1609, 1489, 1198, 1034 cm^{-1}.

*4.1.3.17. N-cyclohexyl-2-(5H-imidazo[5,1-a]isoindol-5-yl)acetamide (**11q**)*

Yield 69.3%. White powder. Mp 84-86 °C. ^{1}H NMR (300 MHz, DMSO-d_6) δ(ppm) 7.98 (d, *J* = 7.8 Hz, 1H), 7.68 (s, 1H), 7.61 (d, *J* = 7.5 Hz, 1H), 7.51 (d, *J* = 7.6 Hz, 1H), 7.39 (t, *J* = 7.4 Hz, 1H), 7.28 (td, *J* = 7.5, 1.2 Hz, 1H), 7.14 (s, 1H), 5.60 (dd, *J* = 9.1, 5.2 Hz, 1H), 2.94 (dd, *J* = 15.1, 5.2 Hz, 1H), 1.63 (ddd, *J* = 64.8, 31.0, 9.4 Hz, 6H), 1.18-1.10 (m, 2H). MS (EI) *m/z* 296.2 $[M+H]^+$. IR (KBr) 3273, 3032, 1653, 1616, 1506, 1260, 1034 cm^{-1}.

*4.1.3.18. 2-(5H-imidazo[5,1-a]isoindol-5-yl)-N-(3-methoxyphenethyl)acetamide (**11r**)*

Yield 78.2%. Yellow powder. Mp 94-96 °C. ^{1}H NMR (300 MHz, Chloroform-*d*) δ(ppm) 7.67 (s, 1H), 7.52 (d, *J* = 7.6 Hz, 1H), 7.43-7.17 (m, 4H), 7.12 (d, *J* = 1.5 Hz, 1H), 6.85-6.69 (m, 3H), 5.91 (d, *J* = 7.2 Hz, 1H), 5.68 (dd, *J* = 9.6, 4.3 Hz, 1H), 3.79 (s, 3H), 3.64 (qd, *J* = 6.9, 3.1 Hz, 2H), 2.93 (d, *J* = 4.4 Hz, 1H), 2.85 (td, *J* = 7.5, 7.0, 2.5 Hz, 2H), 2.42 (dd, *J* = 15.5, 9.5 Hz, 1H). MS (EI) *m/z* 348.2 $[M+H]^+$. IR (KBr) 3273, 3030, 1684, 1595, 1506 cm^{-1}.

*4.1.3.19. 2-(5H-imidazo[5,1-a]isoindol-5-yl)-N-phenethylacetamide (**11s**)*

Yield 77.2%. White powder. Mp 167-169 °C. ^{1}H NMR (300 MHz, Chloroform-*d*) δ(ppm) 7.70 (s, 1H), 7.53 (d, *J* = 7.6 Hz, 1H), 7.43-7.12 (m, 10H), 5.81 (s, 1H), 5.69 (dd, *J* = 9.5, 4.3 Hz, 1H), 3.65 (tt, *J* = 6.7, 3.3 Hz, 2H), 2.92-2.85 (m, 2H), 2.43 (dd, *J* = 15.5, 9.5 Hz, 1H). MS (EI) *m/z* 318.2 $[M+H]^+$. IR (KBr) 3273, 3032, 1653, 1593, 1506 cm^{-1}.

*4.1.3.20. 2-(5H-imidazo[5,1-a]isoindol-5-yl)-N-(2-(pyridin-2-yl)ethyl)acetamide (**11t**)*

Yield 85.2%. White powder. Mp 140-142 °C. ^{1}H NMR (300 MHz, DMSO-d_6) δ(ppm) 8.50 (d, *J* = 4.3 Hz, 1H), 8.21 (s, 1H), 7.83-7.66 (m, 2H), 7.60 (d, *J* = 7.5 Hz, 1H), 7.47 (d, *J* = 7.6 Hz, 1H), 7.38 (t, *J* = 7.4 Hz, 1H), 7.25 (dd, *J* = 14.8, 5.8 Hz, 3H), 7.15 (s, 1H), 5.59 (dd, *J* = 9.3, 5.6 Hz, 1H), 3.54 (q, *J* = 6.5 Hz, 2H), 2.93 (td, *J* = 8.0, 7.2, 3.5 Hz, 2H), 2.55 (d, *J* = 10.0 Hz, 2H). MS (EI) *m/z* 319.2 $[M+H]^+$. IR (KBr) 3273, 3030, 1668, 1593,

1506 cm^{-1}.

*4.1.4 General preparation of intermediates **12a-b***

Different substituted ethan-1-one (1 mol equiv.) was added to a solution of NaOEt (attained from Na (2 mol equiv.) dissolved in EtOH (1.4 M) at 0 °C), followed by the addition of intermediate **6** (1 mol equiv.). The yellow liquid was stirred at room temperature for 3 h. The solvent was removed under reduced pressure and the saturated NH_4Cl solution was added to the mixture to quench the reaction. The mixture was diluted with water, and was extracted with dichloromethane to afford the crude product, which was used to the next step without any further purification.

*4.1.5 General preparation of intermediates **13a-b***

To a solution of **12** (1 mol equiv.) in methyl alcohol (0.2 M) was added AcOH (0.8 M) and the mixture was stirred at 90 °C for 3 h. The mixture was allowed to cool to room temperature and the pH was adjusted to 10 with saturated K_2CO_3 solution. The mixture was evaporated in vacuo to remove methyl alcohol and was extracted with ethyl acetate to afford the crude product that was purified by flash column chromatography on silica gel to yield **13a-b**.

*4.1.5.1 1-cyclohexyl-2-(5H-imidazo[5,1-a]isoindol-5-yl)ethan-1-one (**13a**)*

Yield 50.8%. White powder. Mp 92-94 °C. ^{1}H NMR (300 MHz, Chloroform-*d*) δ(ppm) 7.66 (s, 1H), 7.58-7.53 (dt, *J* = 7.6, 0.9 Hz, 1H), 7.43-7.36 (m, 1H), 7.28-7.21 (m, 2H), 7.28 (s, 1H), 5.73-5.59 (dd, *J* = 9.5, 3.6 Hz, 1H), 3.26-3.16 (dd, *J* = 18.4, 3.6 Hz, 1H), 3.04-2.76 (dd, *J* = 18.4, 9.5 Hz, 1H), 2.49-2.24 (m, 1H), 1.97-1.59 (m, 5H), 1.40-1.19 (m, 5H).

*4.1.5.2 1-(4-chlorophenyl)-2-(5H-imidazo[5,1-a]isoindol-5-yl)ethan-1-one (**13b**)*

Yield 59.9%. White powder. Mp 106-108 °C. ^{1}H NMR (300 MHz, Chloroform-*d*) δ(ppm) 8.01-7.85 (m, 2H), 7.66-7.25 (m, 8H), 6.30 (t, *J* = 7.0 Hz, 1H), 3.43 (dd, *J* = 12.5, 6.9 Hz, 1H), 3.20 (dd, *J* = 12.4, 7.0 Hz, 1H).

*4.1.6 General preparation of compounds **14a-b***

To a solution of **13** (1 mol equiv.) in EtOH at room temperature was added

hydroxylamine hydrochloride (3 mol equiv.) and the solution was stirred at 50 °C overnight. The solvent was removed under reduced pressure to afford the crude product, which was purified by gel chromatography to afford the target products.

*4.1.6.1 (Z)-1-cyclohexyl-2-(5H-imidazo[5,1-a]isoindol-5-yl)ethan-1-one oxime (**14a**)*

Yield 54.2%. White powder. Mp 126-128 °C. ^{1}H NMR (300 MHz, DMSO-d_6) δ(ppm) 8.73 (s, 1H) , 7.81 (s, 1H), 7.70 (s, 1H) , 7.26-7.47 (m, 3H), 7.25 (s, 1H), 5.63-5.66 (m, 1H), 2.98-3.13 (dd, J = 11.4, 6.8 Hz, 2H), 2.87 (s, 1H). 1.64-1.70 (m, 4H), 1.48-1.55 (m, 3H), 1.32-1.42 (m, 3H). MS (EI) *m/z* 296.2 $[M+H]^+$. IR (KBr) 3647, 3033, 1595, 1506 cm^{-1}.

*4.1.6.2 (Z)-1-(4-chlorophenyl)-2-(5H-imidazo[5,1-a]isoindol-5-yl)ethan-1-one oxime (**14b**)*

Yield 49.9%. White powder. Mp 89-91 °C. ^{1}H NMR (300 MHz, Chloroform-*d*) δ(ppm) 9.51 (s, 1H), 7.81 (s, 1H), 7.68 (s, 1H), 7.51-7.41 (m, 7H), 7.35-7.26 (m, 1H), 5.89-5.83 (m, 1H), 3.60-3.52 (dd, J = 12.5, 6.7 Hz, 1H), 3.35-3.27 (dd, J = 11.8, 6.1 Hz, 1H). MS (EI) *m/z* 324.1 $[M+H]^+$. IR (KBr) 3648, 3030, 1595, 1506 cm^{-1}.

4.2. Biology

4.2.1. Hela cell-based enzyme assays

HeLa cells were seeded in 96-well culture plates at a density of $5x10^3$ per well. On the next day, human IFN-γ (100 ng/mL) and compounds in a total volume of 200 μL culture medium containing 15 μg/mL of *L*-tryptophan were added to the cells. After incubation for 24 hours, 140 μL of the supernatant was mixed with 10 μL of 6.1 N trichloroacetic acid and the mixture was incubated for 30 min at 50 °C. The reaction mixture was then centrifuged for 10 minutes at 4000 rpm to remove sediments. 100 μL of the supernatant was mixed with 100 μL of 2% (w/v) *p*-dimethylaminobenzaldehyde in acetic acid and measured at 480 nm. The initial wells containing the cells in the remaining volume of 50 μL were used to estimate cell viability in a classical MTT assay. To that end, 50 μL of culture medium (Iscove medium with 10% FCS and amino acids) were added to the wells together with 20 μL 4 mg/mL of MTT. After 4 h of incubation at 37 ^{o}C, 200 μL

of DMSO were added to dissolve the crystals of formazan blue and the absorbance at 570 nm was measured after overnight incubation at 37 ^{o}C.

4.2.2. Western blot analysis

HeLa cells were seeded in 6-well culture plates at a density of 2x10^5 per well. On the next day, human IFN-γ (100 ng/mL) and compounds in a total volume of 2 mL culture medium were added to the cells. After incubation for 24 hours, the cells were collected and washed with PBS twice. Proteins were extracted from cells by lysis buffer consisting of 50 μM Tris–HCl, pH 8.0, 50 μM KCl, 5 μM DTT, 1 μM EDTA, 0.1% SDS, 0.5% Triton X-100 (Sunshine Biotechnology Co. Ltd.,) and protease inhibitor cocktail tablets (Roche, Indianapolis, IN). The protein lysates were separated by 10% SDS-PAGE and subsequently electrotransferred onto a polyvinylidene difluoride membrane (Millipore, Bedford, MA). The membrane was blocked with 5% nonfat milk for 1 h at room temperature. The blocked membrane was incubated with the indicated primary Abs, and then with a horseradish peroxidase-conjugated secondary Ab. Protein bands were visualized using Western blotting detection system according to the manufacturer's instructions (Cell Signaling Technology, MA).

4.2.3. Measurement of IDO1 absorbance spectra

Absorbance spectra (370-600 nm) were measured immediately after addition of compounds (500 μM) to rhIDO1 (3 μM) in phosphate buffer (pH: 6.5) using Safire multifunctional microplate reader. Changes in the 404 nm maxima indicated binding to the ferric iron of the heme.

4.2.4. T cell proliferation and cytokine assay

T lymphocytes prepared from splenocytes of C57/bl6 mice were resuspended in RPMI 1640 containing 10% FBS, *L*-glutamate, penicillin, and streptomycin. The B16F1 cells were treated with mitomycin C at a final concentration of 25 mg/L and then incubated at 37 °C for 30 min. After being washed three times, the B16F1 cells were resuspended in RPMI 1640 containing 10% FBS, *L*-glutamate, penicillin, and streptomycin. 1×10^5 T

lymphocytes (responder cells) and 2×10^4 mitomycin C treated B16F1 cells (stimulator cells) were added to each well of a 96-well plate in RPMI 1640 containing 10% FBS in the presence of ConA (5 μg/mL). Cell proliferation was quantified by MTT assay. The cells were incubated at 37 °C and 5% CO_2 for 48 h; and 10 μL MTT (4 mg/mL) was added to each well. MTT formazan production was dissolved by DMSO replacing the medium 4 h later. The absorbance at 570 nm (OD570) was measured by a microplate reader. Supernatant collected from the co-culture system were subjected to ELISA analysis for IFN-γ by using kits from Dakawe (Beijing, China).

4.2.5. Treg cell experiments

Tregs were analyzed by using an eBioscience intracellular staining kit according to the manufacturer's instructions. After co-cultured with B16F1 cells, T cells were collected. Surface staining was performed with a $CD4^-$ FITC and $CD25^-$ PE for 15 min at 4 °C. After this, the cells were fixed and permeabilized with fixation buffer and permeabilization wash buffer. The intracellular staining was performed with $FOXP3^-$ APC for 20 min. The cells were then analyzed by flow cytometry analysis.

4.3. Molecular modeling

4.3.1. Induced fit docking

In order to consider the flexibility of both ligand and protein, the *induced fit docking* (IFD) protocol in Schrödinger was employed [44]. In IFD calculations, the ligands were first docked into the rigid receptor using softened energy function in *Glide*. By default, a maximum 20 poses per ligand were retained. Then, the protein degrees of freedom for each complex were sampled and the protein-ligand complexes were minimized. The protein structure in each pose now reflected an induced fit to the ligand structure and conformation. The best protein-ligand complex was then identified based on the predicted binding affinities of the docked ligand. Here, the residues within 5 Å of each of the 20 ligand poses were subjected to a conformational search and energy minimizations, and the residues outside this range were fixed. Finally, the minimized ligand was rigorously redocked into the induced-fit protein structure using *Glide* XP scoring mode, and metal

constraints can be applied to both *Glide* docking stages in IFD protocol. The choice of the best-docked structure for each ligand was made using a model energy score that combines the energy grid score, the binding affinity predicted by GlideScore, and the internal strain energy for the model potential used to direct the conformational-search algorithm.

4.3.2. QM/MM geometry optimization

QM/MM calculations were performed via a two-layer *Qsite* program in Schrödinger [45]. *QSite* is a mixed mode QM/MM program used to study geometries and energies of structures not parameterized for use with molecular mechanics, such as those that contain metal. The reason for this may be complicated. For example, the partial charge of the metal cation is far from being at least approximately constant, and its value might be affected by many factors, for instance by switching the oxidation state of the metal, the nature of the coordinated ligands, the solvation, and/or other environmental factors. Nevertheless, the MM simulation can be basically performed with a reasonable accuracy for a particular coordination sphere when only well-parametrized ligands of the metal interact with the complex surrounding. This is especially the case of a combined QM/MM method where the metal and its closest neighborhood are calculated at the QM level. *QSite* is uniquely equipped to perform QM/MM calculations because it combines the superior speed and power of *Jaguar* with the recognized accuracy of the OPLS force field. *Jaguar* is used for the quantum mechanical part of the calculations [46], and *Impact* provides the molecular mechanics simulation [47]. The QM region is the full heme ring, the Fe, the coordinating His residue and the inhibitor. This subsystem was optimized by employing density functional theory (DFT) using B3LYP with the lacvp* basis set and the convergence criterion for geometry optimizations followed the original *Qsite* defaults [48]. The remaining subsystem was treated with the MM method, and was geometry-optimized by using OPLS-2005 force field. The geometry optimization convergence criterion for MM subsystem was set as RMSD of energy gradient 60 kcal $mol^{-1}Å^{-1}$, and cutoff value was set to 10 Å for non-bonded interactions during the QM/MM calculations. Throughout the QM/MM calculation, the cuts between the QM and MM regions were treated as specially parameterized frozen-orbital boundaries, which was placed between C_α and C_β of

the residue His346.

Acknowledgments

Financial support from the National Natural Science Foundation of China (21472244, 21772233, 21472091 and 81330079) is gratefully acknowledge. This work was also supported by the Jiangsu Province Funds for Distinguished Young Scientists (BK20160033), the Six Major Talent Peak Project of Jiangsu Province (2011-YY-004), and the Fundamental Research Funds for the Central Universities (No. 2015021).

References and notes

[1] G.L. Beatty, W.L. Gladney, Immune escape mechanisms as a guide for cancer immunotherapy, Clin. Cancer Res. 21 (2015) 687–692.

[2] E.P. Tjin, G. Krebbers, K.J. Meijlink, W. van de Kasteele, E.H. Rosenberg, J. Sanders, P.M. Nederlof, B.A. van de Wiel, J.B. Haanen, C.J. Melief, F.A. Vyth-Dreese, R.M. Luiten, Immune-escape markers in relation to clinical outcome of advanced melanoma patients following immunotherapy, Cancer Immunol. Res. 2 (2014) 538–546.

[3] T.S. Johnson, D.H. Munn, Host indoleamine 2,3-dioxygenase: contribution to systemic acquired tumor tolerance, Immunol. Invest. 41 (2012) 765–797.

[4] C. Uyttenhove, L. Pilotte, I. Theate, V. Stroobant, D. Colau, N. Parmentier, T. Boon, B.J. Van den Eynde, Evidence for a tumoral immune resistance mechanism based on tryptophan degradation by indoleamine 2,3-dioxygenase, Nat. Med. 9 (2003) 1269–1274.

[5] I. Théate, N. van Baren, L. Pilotte, P. Moulin, P. Larrieu, J.C. Renauld, C, Hervé, I. Gutierrez-Roelens, E. Marbaix, C. Sempoux, B.J. Van den Eynde, Extensive profiling of the expression of the indoleamine 2,3-dioxygenase 1 protein in normal and tumoral human tissues, Cancer Immunol. Res. 3 (2015) 161–172.

[6] D.H. Munn, M.D. Sharma, B. Baban, H.P. Harding, Y. Zhang, D. Ron, A.L. Mellor, GCN2 kinase in T cells mediates proliferative arrest and anergy induction in response to indoleamine 2,3-dioxygenase, Immunity 22 (2005) 633–642.

[7] F. Fallarino, U. Grohmann, S. You, B.C. McGrath, D.R. Cavener, C. Vacca, C. Orabona, R. Bianchi, M.L. Belladonna, C. Volpi, P. Santamaria, M.C. Fioretti, P. Puccetti, The combined effects of tryptophan starvation and tryptophan catabolites down-regulate T cell receptor zeta-chain and induce a regulatory phenotype in naive T cells, J. Immunol. 176 (2006) 6752–6761.

[8] J.D. Mezrich, J.H. Fechner, X. Zhang, B.P. Johnson, W.J. Burlingham, C.A. Bradfield, An interaction between kynurenine and the aryl hydrocarbon receptor can generate regulatory T cells, J. Immunol. 185 (2010) 3190–3198.

[9] N.T. Nguyen, A. Kimura, T. Nakahama, I. Chinen, K. Masuda, K. Nohara, Y. Fujii-Kuriyama, T. Kishimoto, Aryl hydrocarbon receptor negatively regulates dendritic cell immunogenicity via a kynurenine-dependent mechanism, Proc. Natl. Acad. Sci. U. S. A. 107 (2010) 19961–19966.

[10] C. Sheridan, IDO inhibitors move center stage in immuno-oncology, Nat. Biotechnol. 33 (2015) 321–322.

[11] U.F. Rohrig, S.R. Majjigapu, A. Grosdidier, S. Bron, V. Stroobant, L. Pilotte, D. Colau, P. Vogel, B.J. Van den Eynde, V. Zoete, O. Michielin, Rational design of 4-aryl-1,2,3-triazoles for indoleamine 2,3-dioxygenase 1 inhibition. J. Med. Chem. 55 (2012) 5270–5290.

[12] S. Qian, T. He, W. Wang, Y. He, M. Zhang, L. Yang, G. Li, Z. Wang, Discovery and preliminary structure-activity relationship of 1H-indazoles with promising indoleamine-2,3-dioxygenase 1 (IDO1) inhibition properties, Bioorgan. Med. Chem. 24 (2016) 6194–6205.

[13] A. Coluccia, S. Passacantilli, V. Famiglini, M. Sabatino, A. Patsilinakos, R. Ragno, C. Mazzoccoli, L. Sisinni, A. Okuno, O. Takikawa, R. Silvestri, G. La Regina, New inhibitors of indoleamine 2,3-dioxygenase 1: molecular modelling studies, synthesis and biological evaluation, J. Med. Chem. 59 (2016) 9760–9773.

[14] E.W. Yue, B. Douty, B. Wayland, M. Bower, X. Liu, L. Leffet, Q. Wang, K.J. Bowman, M.J. Hansbury, C. Liu, M. Wei, Y. Li, R. Wynn, T.C. Burn, H.K. Koblish, J.S. Fridman, B. Metcalf, P.A. Scherle, A.P. Combs, Discovery of potent competitive inhibitors of indoleamine 2,3-dioxygenase with in vivo pharmacodynamic activity and efficacy in a mouse melanoma model, J. Med. Chem. 52 (2009) 7364–7367.

[15] U.F. Rohrig, S.R. Majjigapu, M. Chambon, S. Bron, L. Pilotte, D. Colau, B.J. Van den Eynde, G. Turcatti, P. Vogel, V. Zoete, O. Michielin, Detailed analysis and follow-up studies of a high-throughput screening for indoleamine 2,3-dioxygenase 1 (IDO1) inhibitors, Eur. J. Med. Chem. 84 (2014) 284–301.

[16] J.A. Markwalder, S.P. Seitz, Y. Blat, L. Elkin, J.T. Hunt, J.G. Pabalan, M.N. Jure-Kunkel, G.D. Vite, K. Covello, Identification and optimization of a novel series of indoleamine 2,3-dioxygenase inhibitors, Bioorg. Med. Chem. Lett. 27 (2017) 582–585.

[17] E. Dolusic, P. Larrieu, C. Meinguet, D. Colette, A. Rives, S. Blanc, T. Ferain, L. Pilotte, V. Stroobant, J. Wouters, B. Van den Eynde, B. Masereel, E. Delfourne, R. Frederick, Indoleamine 2,3-dioxygenase inhibitory activity of derivatives of marine alkaloid tsitsikammamine A, Bioorg. Med. Chem. Lett. 23 (2013) 47–54.

[18] R. Pasceri, D. Siegel, D. Ross, C.J. Moody, Aminophenoxazinones as inhibitors of indoleamine 2,3-dioxygenase (IDO). Synthesis of exfoliazone and chandrananimycin A, J. Med. Chem. 56 (2013) 3310–3317.

[19] S. Yang, X. Li, F. Hu, Y. Li, Y. Yang, J. Yan, C. Kuang, Q. Yang, Discovery of tryptanthrin derivatives as potent inhibitors of indoleamine 2,3-dioxygenase with therapeutic activity in Lewis lung cancer (LLC) tumor-bearing mice, J. Med. Chem. 56 (2013) 8321–8331.

[20] U.F. Rohrig, S.R. Majjigapu, P. Vogel, V. Zoete, O. Michielin, Challenges in the discovery of

indoleamine 2,3-dioxygenase 1 (IDO1) inhibitors, J. Med. Chem. 58 (2015) 9421–9437.

[21] S. Löb, A. Konigsrainer, H.G. Rammensee, G. Opelz, P. Terness, Inhibitors of indoleamine-2,3-dioxygenase for cancer therapy: can we see the wood for the trees? Nat. Rev. Cancer 9 (2009) 445–452.

[22] E. Vacchelli, F. Aranda, A. Eggermont, C. Sautès-Fridman, E. Tartour, E.P. Kennedy, M. Platten, L. Zitvogel, G. Kroemer, L. Galluzzi, Trial watch: IDO inhibitors in cancer therapy, Oncoimmunology 3 (2014) e957994.

[23] M. Mautino, F. Jaipuri, J. Waldo, S. Kumar, J. Adams, C. Van Allen, A. Marcinowicz-Flick, D. Munn, N. Vahanian, C.J. Link, Abstract 491: NLG919, a novel indoleamine-2,3-dioxygenase (IDO)-pathway inhibitor drug candidate for cancer therapy, AACR 2013.

[24] J. Spahn, J. Peng, E. Lorenzana, D. Kan, T. Hunsaker, E. Segal, M. Mautino, E. Brincks, A. Pirzkall, S. Kelley, S. Mahrus, L. Liu, S. Dale, C. Quiason, E. Jones, Y. Liu, S. Latham, L. Salphati, K. DeMent, M. Merchant, G. Hatzivassiliou, Improved anti-tumor immunity and efficacy upon combination of the IDO1 inhibitor GDC-0919 with anti-PD-L1 blockade versus anti-PD-L1 alone in preclinical tumor models, J. ImmunoTherapy Cancer 3 (2015) 303.

[25] https://www.clinicaltrials.gov/ct2/results?term=GDC0919&Search=Search

[26] Y.H. Peng, S.H. Ueng, C.T. Tseng, M.S. Hung, J.S. Song, J.S. Wu, F.Y. Liao, Y.S. Fan, M.H. Wu, W.C. Hsiao, C.C. Hsueh, S.Y. Lin, C.Y. Cheng, C.H. Tu, L.C. Lee, M.F. Cheng, K.S. Shia, C. Shih, S.Y. Wu, Important hydrogen bond networks in indoleamine 2,3-dioxygenase 1 (IDO1) inhibitor design revealed by crystal structures of imidazoleisoindole derivatives with IDO1, J. Med. Chem. 59 (2015) 282–293.

[27] Y. Zou, J. Xiao, Z. Tu, Y. Zhang, K. Yao, M. Luo, K. Ding, Y. Zhang, Y. Lai, Structure-based discovery of novel 4,5,6-trisubstituted pyrimidines as potent covalent Bruton's tyrosine kinase inhibitors, Bioorg. Med. Chem. Lett. 26 (2016) 3052–3059.

[28] E.W. Yue, R. Sparks, P. Polam, D. Modi, B. Douty, B. Wayland, B. Glass, A. Takvorian, J. Glenn, W. Zhu, M. Bower, X. Liu, L. Leffet, Q. Wang, K.J. Bowman, M.J. Hansbury, M. Wei, Y. Li, R. Wynn, T.C. Burn, H.K. Koblish, J.S. Fridman, T. Emm, P.A. Scherle, B. Metcalf, A.P. Combs, INCB24360 (Epacadostat), a Highly Potent and Selective Indoleamine-2,3-dioxygenase 1 (IDO1) Inhibitor for Immuno-oncology, ACS Med. Chem. Lett. 8 (2017) 486–491.

[29] S. Tojo, T. Kohno, T. Tanaka, S. Kamioka, Y. Ota, T. Ishii, K. Kamimoto, S. Asano, Y. Isobe, Crystal structures and structure-activity relationships of imidazothiazole derivatives as IDO1 inhibitors, ACS Med. Chem. Lett. 5 (2014) 1119–1123.

[30] Y. Zou, Y. Wang, F. Wang, M. Luo, Y. Li, W. Liu, Z. Huang, Y. Zhang, W. Guo, Q. Xu, Y. Lai, Discovery of potent IDO1 inhibitors derived from tryptophan using scaffold-hopping and structure-based design approaches, Eur. J. Med. Chem. 138 (2017) 199–211.

[31] Y. Zou, F. Wang, Y. Wang, W. Guo, Y. Zhang, Q. Xu, Y. Lai, Systematic study of imidazoles inhibiting IDO1 via the integration of molecular mechanics and quantum mechanics calculations, Eur. J. Med. Chem. 131 (2017) 152–170.

[32] M. Mautino, S. Kumar, J. Waldo, F. Jaipuri, T. Kesharwani. Fused imidazole derivatives useful as IDO inhibitors, 2012. PCT Int. Appl. WO2012142237.

[33] A. Richard, B. Matilda, P. Thomas, G. Camille. 4H-imidazo[1,5-*a*]indole derivatives and their use as indoleamine 2,3-dioxygenase (IDO) and/or tryptophan 2,3-dioxygenase (TDO2) modulators, 2016. PCT Int. Appl. WO2016051181.

[34] B.A. Sherer. Cyclohexyl-ethyl substituted diaza- and triaza-tricyclic compounds as indoleamine 2,3-dioxygenase (IDO) antagonists for the treatment of cancer, 2016. PCT Int. Appl. WO2016037026.

[35] E.W. Yue, B. Douty, B. Wayland, M. Bower, X. Liu, L. Leffet, Q. Wang, K.J. Bowman, M.J. Hansbury, C. Liu, M. Wei, Y. Li, R. Wynn, T.C. Burn, H.K. Koblish, J.S. Fridman, B. Metcalf, P.A. Scherle, A.P. Combs, Discovery of potent competitive inhibitors of indoleamine 2,3-dioxygenase with in vivo pharmacodynamic activity and efficacy in a mouse melanoma model, J. Med. Chem. 52 (2009) 7364–7367.

[36] M. Sono, T. Taniguchi, Y. Watanabe, O. Hayaishi, Indoleamine 2,3-dioxygenase. Equilibrium studies of the tryptophan binding to the ferric, ferrous, and CO-bound enzymes, J. Biol. Chem. 255 (1980) 1339–1345.

[37] D.H. Munn, Blocking IDO activity to enhance anti-tumor immunity. Front. Biosci. 4 (2012) 734–745.

[38] P. Hwu, M.X. Du, R. Lapointe, M. Do, M.W. Taylor, H.A. Young, Indoleamine 2,3-dioxygenase production by human dendritic cells results in the inhibition of T cell proliferation, J. Immunol. 164 (2000) 3596–3599.

[39] T.M. Bauer, L.P. Jiga, J.J. Chuang, M. Randazzo, G. Opelz, P. Terness, Studying the immunosuppressive role of indoleamine 2,3-dioxygenase: tryptophan metabolites suppress rat allogeneic T-cell responses in vitro and in vivo, Transplant Int. 18 (2005) 95–100.

[40] D.B. Kitchen, H. Decornez, J.R. Furr, J. Bajorath, Docking and scoring in virtual screening for drug discovery: methods and applications, J. Nat. Rev. Drug Discov. 3 (2004) 935–949.

[41] H.A. Carlson, J.A. McCammon, Accommodating protein flexibility in computational drug design, Mol. Pharmacol. 57 (2000) 213–218.

[42] F. Šebesta, V. Sláma, J. Melcr, Z. Futera, J.V. Burda, Estimation of transition-metal empirical parameters for molecular mechanical force fields, J. Chem. Theory Comput. 12 (2016) 3681–3688.

[43] A. Warshel, M. Levitt, Theoretical studies of enzymic reactions: dielectric, electrostatic and steric stabilization of the carbonium ion in the reaction of lysozyme, J. Mol. Biol. 103 (1976) 227–249.

[44] Induced Fit Docking protocol, Glide version 5.5, Prime version 2.1, Schrödinger, LLC, New York, NY, 2009.

[45] QSite, version 5.1, Schrödinger, LLC, New York, NY, 2009.

[46] Jaguar, version 7.6, Schrödinger, LLC, New York, NY, 2009.

[47] Impact, version 5.5, Schrödinger, LLC, New York, NY, 2009.

[48] P.J. Hay, W.R. Wadt, Ab initio effective core potentials for molecular calculations. Potentials for K to Au including the outermost core orbitals, J. Chem. Phys. 82 (1985) 299–310.

Highlights:

- The extensive structural modification of GDC-0919 analogue was explored.
- T-lymphocytes assays were performed to evaluate the capacity of the compounds in the reversal of IDO1-mediated immunosuppression.
- UV spectra provided a direct evidence of our compounds binding to the active site of IDO1.
- Molecular simulations were performed to predict the binding mode of our compounds.